Earth and Planetary Science Letters 414 (2015) 176–186

Contents lists available at ScienceDirect

Earth and Planetary Science Letters

www.elsevier.com/locate/epsl

Incoming plate faulting in the Northern and Western Pacific and implications for subduction zone water budgets

Erica L. Emry *,[1], Douglas A. Wiens

Department of Earth and Planetary Sciences, Washington University in St. Louis, Campus Box 1169, One Brookings Drive, St. Louis, MO 63130, USA

ARTICLE INFO

Article history:
Received 30 August 2014
Received in revised form 17 December 2014
Accepted 22 December 2014
Available online xxxx
Editor: P. Shearer

Keywords:
pacific plate
incoming plate faulting
subduction zone trench
serpentinite

ABSTRACT

The greatest uncertainty in the amount of water input into the Earth at subduction zones results from poor constraints on the degree of mantle serpentinization in the incoming plate. Recent studies suggest that the depth of serpentinization within the incoming plate mantle is likely controlled by the depth of extensional faulting caused by lithospheric bending at the outer rise and trench. We explore the maximum depth of extension within the incoming plate at Northwestern Pacific subduction zones in order to estimate the depth limit of serpentinization and to identify any significant variation between subduction zone segments. We relocate trench earthquakes to identify which events occurred within the incoming plate and determine accurate depths for 63 incoming plate earthquakes occurring during 1988–2011 by inverting teleseismic broadband P and SH waveforms. We observe that the top 10–15 km of the incoming plate mantle experiences extensional faulting at all of the subduction zones with a reasonable sample of earthquakes; 60% of the total number of extensional earthquakes occur at crustal depths or within the top 5 km of the incoming plate mantle, 80% occur above 10 km within the mantle, and 95% occur above 15 km. There is evidence for variation throughout the different regions of study, for example extensional earthquakes occur down to 20 km below the crust in the western Aleutians and Izu–Bonin. We propose that the incoming plate mantle is most strongly hydrated in the upper 5 km, and that partial serpentinization exists regionally within the incoming plate mantle to ~15 km. Making reasonable assumptions about the degree of serpentinization and incorporating previous estimates of crustal water, we calculate that the total water carried into the Northern and Western Pacific subduction zones is generally higher than previous estimates, and is approximately 4–6 $\times 10^8$ Tg/Myr, or ~45–70 $\times 10^3$ Tg/Myr per kilometer of subduction zone.

1. Introduction

Prominent extensional faulting within the incoming plates at subduction zone trenches may provide a pathway by which seawater can enter the plate down to mantle depths and hydrate dry mantle rocks prior to subduction. In this case, large amounts of mantle serpentinite within the incoming plate may significantly impact subduction zone and upper mantle water budgets (e.g. Ranero et al., 2003). Mantle serpentinites within the subducting slab can remain colder and thus more stable to greater depths than crustal hydrated rocks and therefore may significantly contribute to water flux from the slab at intermediate and deep depths (e.g. Jarrard, 2003; Hacker, 2008; Van Keken et al., 2011). Depending on the subduction zone, this could impact island arc and back arc basin volcanism (e.g. Kelley et al., 2006) or the amount of water carried deeper into the Earth's mantle (e.g. Rüpke et al., 2004; Hirschmann, 2006).

Surveys of faults, seismicity and seismic tomography at the same region of the Nicaragua incoming plate show that deep extensional faults are continuous from the surface to mantle depths (Ranero et al., 2003), that locally-detected extensional earthquakes occur down to ~6–9 km within the mantle (Lefeldt et al., 2009), and that regions of slow mantle P-wave velocities extend to roughly 10 km deep within the mantle in some regions (Ivandic et al., 2010; Van Avendonk et al., 2011; Lefeldt et al., 2012). The estimates of mantle hydration from Van Avendonk et al. (2011) from seismic tomography extend slightly deeper than the depth estimate for the neutral plane (maximum depth of extensional earthquakes) from small, locally-recorded earthquakes Lefeldt et al. (2009, 2012); however this difference may be explained by the effect of seismic anisotropy on P-wave velocities or by the effect of plate interface seismic cycle on the short-term stress distribution within the incoming plate (Van Avendonk et al., 2011).

* Corresponding author.
E-mail address: ele11@psu.edu (E.L. Emry).
[1] Now at: Department of Geosciences, Pennsylvania State University, 407 Deike Building, University Park, PA 16802, USA.

http://dx.doi.org/10.1016/j.epsl.2014.12.042
0012-821X/

Despite small differences between the studies, it is clear that the region of the slowest observed mantle P-wave velocities (and the greatest amount of mantle hydration) extends to depths that are generally consistent with the observed depth of normal faulting (Lefeldt et al., 2009). Although there is compelling evidence for serpentinites within the mantle of incoming ocean plates, the mechanism by which water is brought to depth in the incoming plate in order to hydrate dry mantle peridotites, is uncertain. Many mechanisms have been proposed (Sibson, 1994; Phipps Morgan and Holtzman, 2005; Korenaga, 2007); most recently Faccenda et al. (2009) proposed that the increasing curvature of the slab as it nears the trench and begins to subduct creates subhydrostatic pressures within the crust and uppermost mantle, pulling water from hydrated regions through fractures and deeper into the incoming plate.

A significant percentage of material subducted into the mantle descends at Northwest Pacific subduction zones, and most of these regions lack the detailed local surveys such as described above for Central America. As Hacker (2008) and Van Keken et al. (2011) highlight from numerical models, flux of water from the subducting slab is dependent on several variables including the hydration state, temperature and convergence rate of the subducting slab. The Northern and Western Pacific oceanic plate is converging at a moderate rate, yet it also is subducting some of the oldest and coldest oceanic lithosphere on Earth. Most of the Northern and Western Pacific subduction zones have experienced large extensional incoming plate earthquakes during instrumental and historic records (Kanamori, 1971; Abe, 1972; Lay et al., 2009). Similar to results from Van Avendonk et al. (2011) that show regions of slow seismic velocities varying in depth within the incoming plate between Nicaragua and Costa Rica, we expect that varying amounts of faulting and subsequent hydration of the Northern and Western Pacific subduction zones may contribute to regional differences in mantle wedge water contents, occurrence of intermediate depth earthquakes, and possibly even mantle transition zone water concentrations.

In this paper, we focus on incoming plate earthquakes at Northern and Western Pacific subduction zones spanning from the Alaska–Aleutian system to the Izu–Bonin subduction zone. These earthquakes have often been termed “outer rise” in the seismological literature, but in fact many of them occur beneath the trench axis, so we prefer the term “incoming plate” earthquakes. Although the International Seismic Centre (ISC) systematically determines earthquake depths, depths determined from teleseismic phase arrival picks are subject to large uncertainties (see Supplementary Figs. S2, S3). Additionally, depths determined by the Global Centroid Moment Tensor (GCMT) catalog for their moment tensor inversion are determined using long period waveforms and are subject to significant uncertainties and trade-offs at shallow depths, so shallow earthquake depths are often fixed at $\sim$15 km. Many of these incoming plate regions have been evaluated separately in event-specific studies (Table S1); however we present a systematic analysis spanning a larger time period at regions with varying tectonic characteristics and compare and contrast our observations throughout the entire Northern and Western Pacific region. We estimate the extent of serpentinization within the incoming oceanic plate from the depth of incoming plate extensional faulting, how hydration may vary throughout these subduction zones, and discuss how these patterns may impact subduction zone processes and the global water budget.

2. Data sets and methods

2.1. Earthquake relocation

We first relocated all GCMT earthquakes that occur near the subduction trench axis; we do this in order to help distinguish earthquakes that occur along the shallow thrust plate interface from those that occur within the incoming plate (Emry et al., 2014). Arrival time data for all GCMT earthquakes occurring in the Western and Northern Pacific during January 1976–July 2011 were collected from the International Seismic Center (ISC) Bulletin (2010). All GCMT earthquakes occurring within 60 km landward of the trench axis or occurring at any distance seaward of the trench were split into separate groups for relocation. We divide earthquakes by region in order to ensure that travel times of all events are affected by a roughly similar Earth structure. The divisions used to separate events were based on spatial distributions of events prior to relocation and are listed in Table S2.

We used the hypocentroidal decomposition relative relocation algorithm (Jordan and Sverdrup, 1981) to relocate groups of earthquakes. Initial earthquake locations were taken from the ISC bulletin (2010). Travel times for P, pP, PKP, and S phases from each event were calculated from the IASP91 earth model (Kennett and Engdahl, 1991). S phases for stations farther than 20° to the earthquake hypocenter were omitted due to generally larger arrival time uncertainties. The total number of earthquakes relocated in each group is listed in Table S2.

The epicentral locations and the lateral relationships between the events aid us somewhat in deciding whether events are shallow thrust or within the incoming plate, but subsequent waveform inversions are not reliant upon the relocated event depths as we employ a grid search and forward modeling of waveforms. If the setting of the earthquake (shallow thrust, incoming plate) was questionable, we continued with the waveform inversion in order to correctly identify the type of earthquake source. The differences between our locations and other catalogs are discussed in the supplementary, but overall we find the differences to be too small to significantly affect our depth determinations, given the 30–90° distances to seismic stations. The final set of earthquakes analyzed in this paper are shown in Fig. 1 and listed in Table 1.

2.2. Waveform inversion

Following relocation, we use teleseismic P- and SH-waveform inversion to determine best fitting source parameters for moderate-sized earthquakes located on the incoming plate or near the trench axis. We obtained waveform data from Global Seismograph Network (GSN) stations through the IRIS DMC (www.iris.edu) for all events greater than Mw 5.5 occurring after 1990, for two events greater than Mw 6.0 occurring prior to 1990, and for events with Mw 5.0–5.5. Using the GSN data, we first tested the lower magnitude (5.0–5.5) events for high signal to noise ratio (SNR), as discussed below, and if high SNR was found, additional data from other global stations were requested. We did not request any data for earthquakes closely resembling shallow thrust events (located notably landward of the trench axis, shallow dip $\lesssim$25°, oriented perpendicular to plate convergence, slip angle $\sim$90°). As mentioned above, if the event could not be identified as distinctly incoming plate or shallow thrust, we proceeded with the waveform inversion. Of 8 ambiguous events, following waveform inversion, 5 were interpreted to be shallow thrust events and 3 were identified as occurring within the incoming plate.

Waveforms for Mw 5.0–5.4 incoming plate earthquakes were tested to find events with sufficient signal to noise ratio (SNR) at the frequency range used in this study from GSN broadband data. For each event, instrument response was removed, and SNR was determined for three passbands: 0.02–0.5 Hz, 0.02–0.2 Hz, and 0.02–0.18 Hz. For each passband, the SNR was computed using three methods within the SEIZMO MATLAB package (*Euler*, https://github.com/g2e/seizmo): peak-to-peak amplitude, root-mean-square (RMS), and the ratio of peak-to-peak signal amplitude vs. noise RMS. The time window used for noise was 50–10 s prior

Table 1
New locations and depths (this study).

Event	Date	Time (UTC)	Latitude (° North)	Longitude (° East)	Depth[a,b] (km)	Time func. (s)	Mw	Event type[c]	Top freq. (Hz)	# of Wvfms.	Misfit[d]
Alaska–Aleutian											
1	16 Jan 1999	10:44:42.90	56.3538	−147.2899	26.5 ± 2	2	5.93	C	0.5	45	0.2858
2	23 Jan 2000	08:42:29.10	57.6226	−149.0905	4.5 ± 2	1	5.52	SS	0.5	21	0.6425
3	27 Sept 1992	17:48:12.96	53.7911	−157.4670	9.5 ± 2	2	5.87	N	0.5	29	0.4072
4	3 May 2010	14:04:23.70	52.5430	−163.6016	9.5 ± 1	1	5.46	N	0.5	22	0.4886
5	7 Aug 2004	09:30:17.98	51.7127	−166.3158	8.5 ± 1	4	6.00	N	0.5	50	0.3191
6	4 May 1994	11:47:23.12	51.5844	−168.5367	12.5 ± 2	1	5.43	N	0.5	10	0.6913
7	28 Dec 2002	09:36:12.73	51.5603	−168.5633	10.5 ± 2	1	5.49	N	0.5	37	0.4294
8	14 Apr 1993	05:58:34.24	51.1857	−168.8008	10.5 ± 2	3	5.95	N	0.5	29	0.3522
9	19 Aug 1992	00:57:41.81	50.5824	−174.9484	13.5 ± 2	3	6.08	N	0.5	32	0.2557
10	15 Apr 1992	05:35:04.50	50.3010	−176.0652	10.5 ± 2	2	5.53	N–SS	0.5	30	0.3999
11	26 June 2006	01:59:17.20	50.3040	−176.1655	9.5 ± 2	2	5.41	N	0.5	46	0.4056
12	11 Nov 1993	00:28:36.38	50.3164	−177.4839	24.5 ± 2	3	5.95	N	0.5	37	0.3496
13	15 Aug 2007	20:22:13.32	50.3687	−177.5885	8.5 ± 2	3	6.41	N	0.5	42	0.2430
14	2 Sept 1999	02:33:37.56	50.7070	−177.6827	8.5 ± 2	2	5.34	SS	0.4	31	0.5077
15	6 July 2009	14:53:12.71	50.4593	177.0526	30.5 ± 3	1	6.05	N–SS	0.5	22	0.4674
16	7 Feb 1988	18:15:07.40	50.8566	173.4344	9.5 ± 4	6	6.38	N	0.18	25	0.3632
17	12 Feb 1997	05:19:04.70	52.1393	171.2434	8.5 ± 1	1	5.51	N	0.5	27	0.4656
18	4 Aug 2006	07:45:49.69	52.1743	171.0589	11.5 ± 1	1	5.49	N	0.5	20	0.3610
Kamchatka											
19	18 May 2011	17:42:36.55	55.4763	163.8497	16.5 ± 2	1	5.50	N	0.5	44	0.5691
20	26 Nov 1999	00:29:01.84	55.2337	165.3382	21 ± 3	2	6.06	SS	0.5	37	0.4301
21	11 Apr 1989	03:56:37.29	49.5404	159.0874	9.5 ± 2	8	6.71	N	0.18	42	0.2338
22	10 Aug 2005	12:47:39.77	48.6982	158.0978	42 ± 2	1	5.38	C	0.5	40	0.5105
Kuril											
23	28 May 1992	21:24:51.36	47.6389	155.3989	7 ± 2	2	5.58	N	0.5	47	0.6191
24	17 Nov 2006	04:09:55.38	47.0563	155.4486	4 ± 1	2	5.53	N	0.5	32	0.5628
25	17 Nov 2006	06:33:50.32	47.0434	155.5093	4 ± 1	1	5.43	N	0.5	33	0.6512
26	15 Nov 2006	19:25:26.56	47.0323	154.9654	3 ± 1	1	5.65	N	0.5	33	0.5234
27	13 Jan 2007	17:37:07.41	46.9146	156.2605	17 ± 2	3	6.01	N–SS	0.5	38	0.3017
28	5 Sept 1994	22:13:48.95	46.8178	155.1344	9 ± 2	1	5.55	N–SS	0.5	41	0.4620
29	24 Nov 2006	15:34:11.04	46.7845	153.7519	10 ± 2	1	5.61	N	0.5	50	0.4755
30	16 Nov 2006	06:20:21.76	46.3528	154.4874	10 ± 1	2	6.00	N	0.5	50	0.4774
31	7 Dec 2006	19:10:21.77	46.1696	154.3725	10 ± 2	4	6.37	N	0.5	50	0.3940
32	13 Sept 2004	03:00:14.75	43.8884	151.3214	4 ± 1	3	5.97	N	0.5	44	0.3634
33	6 Feb 2003	18:48:40.02	43.1867	147.9108	23 ± 5	4	5.57	N–SS	0.5	37	0.5450
Northern Japan											
34	7 May 1991	13:09:31.72	39.4835	144.6595	20 ± 2	1	5.99	N	0.5	19	0.2614
35	5 May 2011	14:58:20.68	38.2463	144.0672	18 ± 5	3	5.96	N	0.5	50	0.5610
36	14 Nov 2005	21:38:51.86	38.1550	144.9285	12 ± 2	9	7.01	N	0.5	50	0.2013
37	17 Jan 2010	06:04:37.92	37.9833	143.5729	24 ± 2	3	5.57	SS	0.5	44	0.3325
38	18 Mar 2011	03:23:55.61	37.8227	143.5179	15 ± 3	1	5.62	N	0.5	45	0.5685
39	9 May 2011	20:15:55.89	37.8124	143.5359	13 ± 2	1	5.70	N	0.5	44	0.5852
40	17 Mar 2011	06:12:40.49	37.7967	143.4238	7 ± 3	7	5.73	N	0.5	32	0.4920
41	14 June 2011	13:06:54.78	37.7940	143.5197	16 ± 3	1	5.80	N–SS	0.5	50	0.6431
42	12 Mar 2011	12:53:50.52	37.7827	143.5197	20 ± 3	3	5.96	N	0.5	44	0.6171
43	3 June 2011	00:05:05.29	37.3472	143.9234	14 ± 3	3	6.15	N–SS	0.5	50	0.3819
44	22 Mar 2011	07:18:47.55	37.2562	144.1037	10 ± 1	5	6.45	N	0.5	50	0.2398
45	22 Mar 2011	12:01:21.94	36.8978	143.2142	22 ± 4	2	5.76	N	0.5	29	0.7258
46	17 Aug 2011	11:44:09.36	36.8189	143.7666	8 ± 2	3	6.22	N	0.5	50	0.3291
47	14 Mar 2011	03:15:53.22	36.3166	142.0871	13 ± 3	2	5.47	C	0.5	33	0.5575
48	13 Mar 2011	01:26:06.28	35.7527	141.6793	19 ± 3	4	6.26	N	0.5	49	0.4761
Izu–Bonin											
49	24 May 1997	05:15:39.27	33.7168	142.0872	9 ± 2	1	5.33	N–SS	0.5	21	0.5172
50	29 July 2005	20:25:03.96	33.4587	142.3966	4 ± 1	4	5.55	N	0.5	47	0.4072
51	27 July 2005	02:39:22.51	33.4050	142.3880	3 ± 1	1	5.41	N	0.5	43	0.5988
52	25 Oct 1999	07:29:58.65	32.1033	142.2747	11 ± 3	2	5.87	N	0.5	41	0.5820
53	5 Jan 2011	00:57:31.69	31.6720	142.2905	10 ± 1	1	5.63	N	0.5	49	0.5919
54	2 Nov 2004	08:46:00.58	28.8189	143.2545	10 ± 1	3	5.74	N–SS	0.5	35	0.4334
55	4 Mar 2002	20:21:23.42	28.5644	143.3213	9 ± 2	1	5.51	N	0.5	39	0.5664
56	1 June 2003	17:50:26.96	28.2978	142.8072	9 ± 2	2	5.62	N	0.5	45	0.4803
57	6 Nov 1996	20:01:02.53	28.1193	143.5693	12 ± 1	4	6.46	N–SS	0.5	47	0.2557
58	21 Dec 2010	17:19:41.19	26.9231	143.7696	18 ± 2	6	7.18	N–SS	0.5	50	0.2533
59	15 June 2011	04:40:59.72	26.8284	144.1564	5 ± 1	3	5.52	N	0.5	48	0.3428
60	22 Dec 2010	21:49:41.05	26.8056	143.6767	29 ± 5	2	6.40	SS	0.5	50	0.5870
61	22 Dec 2010	01:31:20.03	26.7521	143.5144	8 ± 1	4	5.65	N–SS	0.5	22	0.4356
62	6 Aug 2006	18:16:40.48	26.1467	144.0780	24 ± 1	2	5.92	N	0.5	50	0.2439
63	9 Feb 2005	18:46:10.91	26.1019	144.1007	26 ± 2	5	6.31	N	0.5	50	0.2126

[a] Denotes depth beneath seafloor (depth within plate).
[b] Depth uncertainty calculated as depth difference where the misfit is 5% more than the best-fitting model, as in Emry et al. (2014).
[c] SS – strike-slip; C –compression; N – extensional; ST – shallow thrust.
[d] Misfit is measured as the squared amplitude error.

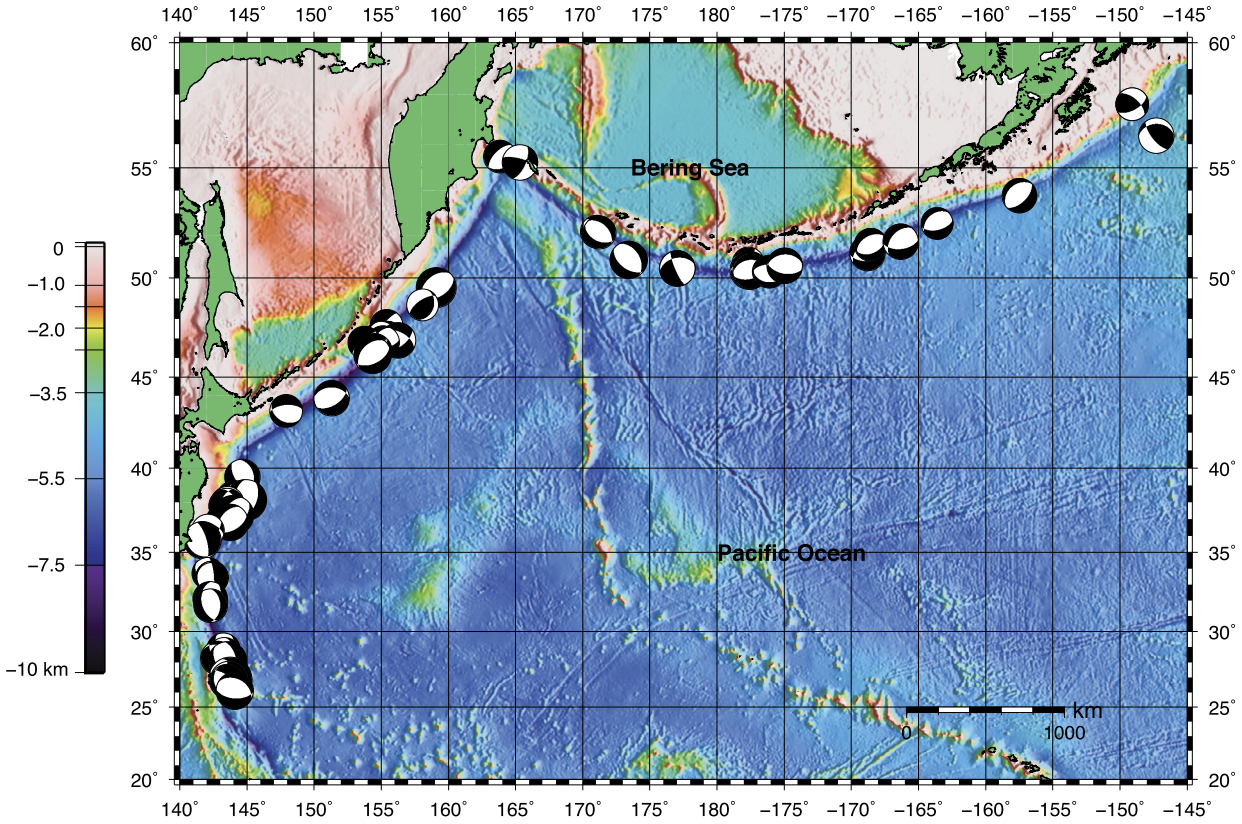

Fig. 1. Focal mechanisms of the studied earthquakes near the trench axes of Northern and Western Pacific subduction zones. Black focal mechanisms correspond to events on Table 1 and are relocated GCMT earthquakes for which new depths are inverted. Throughout the paper, all plotted focal mechanisms in map-view are lower-hemisphere projections with compressional quadrants shown in black or gray and dilatational quadrants are shown in white. Depth of seafloor corresponds to the colorbar on the left.

to the P- and S-arrival times calculated according to the TauP travel time calculator (Crotwell et al., 1999), and the window for signal was 10 s prior to the estimated arrival to 40 s following. The SNR for P-wave arrivals were determined from the vertical component and the SNR for S-wave arrivals were determined from the horizontal components. Events with 10+ P or S traces with SNR 5+ were further analyzed. This criterion was based on the peak-to-peak signal vs. peak-to-peak noise of the 0.02–0.5 Hz pass band. We use this SNR criterion, because the waveforms for Mw 5.5+ events in this study and in Emry et al. (2014) were visually inspected for high SNR – an approach that resembles peak-to-peak SNR.

Broadband data were used for most earthquakes in this study; for two events occurring before 1990, broadband and long-period data were used. Although most Mw 5.5+ earthquakes after 1990 have high SNRs at a sufficient number of stations, a few were omitted, either due to low SNRs (determined visually) within the 0.02–0.5 Hz passband or because long period signal from prior large events overwhelmed signal from the earthquake. Many Mw 5.5+ events had sufficient signal to invert using only GSN-broadband stations, although where necessary additional data were requested; for most Mw 5.0–5.5 events, additional waveform data were requested. All waveforms were recorded at 30–90° from the GCMT earthquake source. Waveforms were visually checked for clear signals at 0.02–0.5 Hz, and instrument responses from the IRIS DMC were deconvolved prior to fitting the synthetics.

We use the ray theory method (e.g. Langston and Helmberger, 1975) and the ray parameter that corresponds to teleseismic propagation to the station using the IASP91 model to compute our synthetic waveforms (Emry et al., 2014). Synthetics were first calculated for three fundamental double-couple source geometries and then combined to obtain synthetics for each focal mechanism tested within the grid search. A ray expander routine was used to compute all the reflections and conversions in the near-source structure model above a cut-off amplitude, and the duration of the source time function, which was modeled as a half sine, was determined within the grid search. The 1-d average shallow velocity structures used to compute synthetics were estimated from active source refraction experiments and are listed in Table S3. Fig. S1 shows an example of waveforms and matching synthetics for an incoming plate earthquake at the Aleutian trench.

A thorough discussion of the waveform modeling method as well as uncertainties in estimated depths are available at length in Emry et al. (2014), however, we briefly discuss here the contributions to uncertainty for our depths. The first contributing factor is the goodness of fit between the modeled waveform and the data, which is dependent upon having a high data SNR from several stations at many backazimuths. To address the first contribution to uncertainty (modeled waveform fits) in Emry et al. (2014), we assigned uncertainties based on the depth at which the calculated misfit was 5% greater than the best-fitting solution – allowing us to identify which events had better constrained depths relative to the others in the group. For consistency, we compute uncertainties in the same manner as in Emry et al. (2014), and the results are included in Table 1.

The second contributing factor is the assumed source-side velocity model: the thickness of the crustal layers and the velocities assumed for the crust and upper mantle. We attempted to limit this error by using velocity models from active-source refraction seismology rather than a global average model for oceanic crust; however, generally only one refraction survey had been completed over the incoming plate at the subduction zones of interest (Table S3). Given a reasonable range for the thickness of the crust and the seismic velocities assumed, we reasoned in Emry et al. (2014)

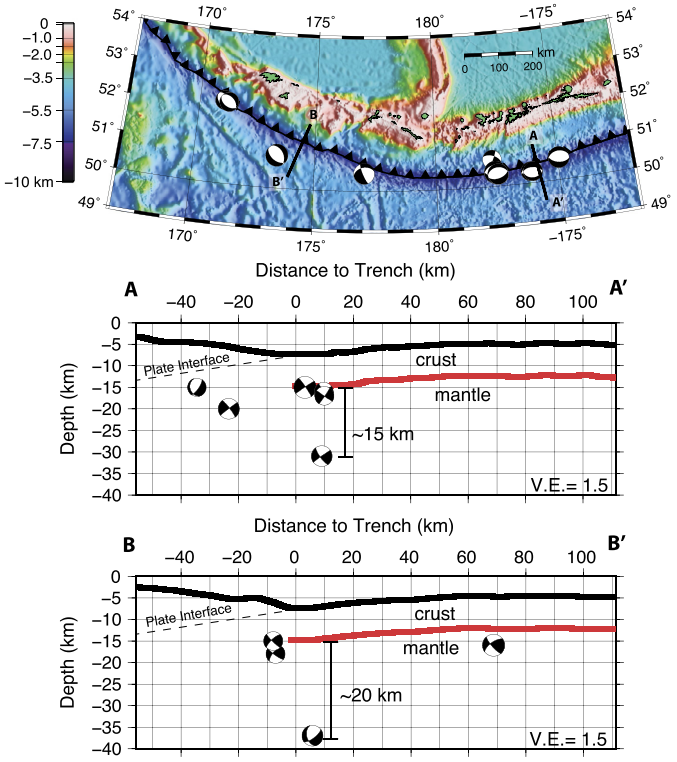

Fig. 2. Top: Map view of the Central and Western Aleutian Trench showing the location of earthquakes for which depths were inverted in this paper. Solid black lines show the locations of the cross-sectional profiles below. **Bottom:** Cross-section near the Andreanof and Delarof Islands showing the distance and depth of studied earthquakes. The thick black line shows bathymetry; the thick red line shows the boundary between the crust and mantle (Moho) as input into our waveform inversion. All focal-mechanisms plotted in cross-sectional view in this paper are rotated 90° from their map-view orientation. **Bottom:** Cross-section at the Rat and Near Islands in the Western Aleutians similar to above. (For interpretation of the references to color in this figure legend, the reader is referred to the web version of this article.)

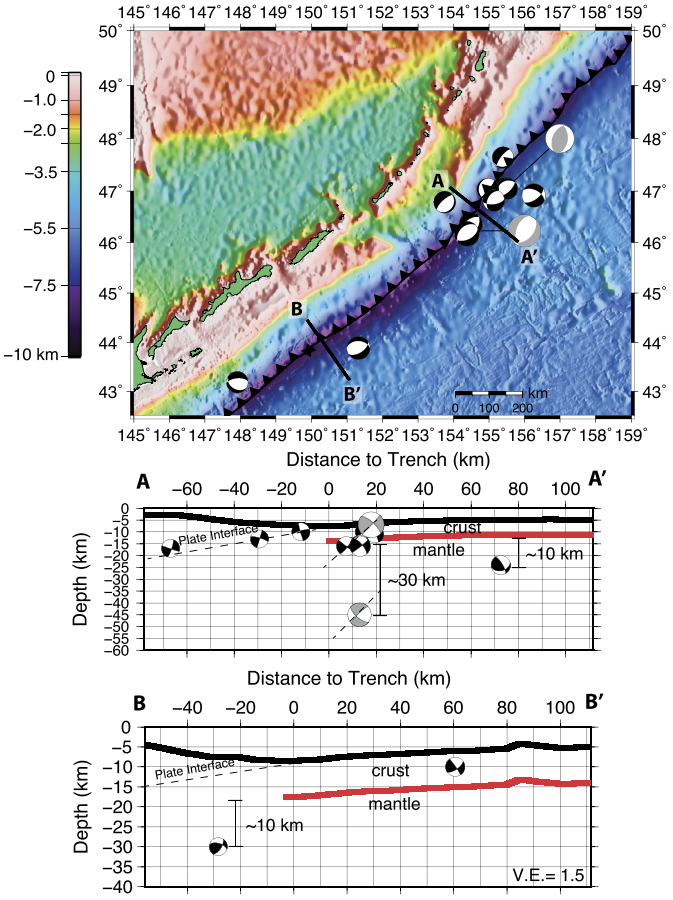

Fig. 3. Top: Map view of the Kuril Islands showing relocated earthquakes with newly determined depths. Fault parameters for two large events from 2007 and 2009 are also plotted (in gray) with dashed tie lines pointing to their locations (Lay et al., 2009). **Middle:** Cross-section near the Northern Kuril Islands showing the distance and depth of earthquakes in this study (colors and focal mechanisms are plotted as in Fig. 2). Gray and white focal mechanisms correspond to the two large 2007 and 2009 outer rise events with fault parameters and fault plane dimensions as modeled by Lay et al. (2009). **Bottom:** Cross-section near the Southern Kuril Islands similar to above.

that about 1–2 km of uncertainty could result from having an inaccurately known incoming plate velocity model, given the depths at which the majority of our crustal and uppermost mantle events occurred. However, for only a few events in our results that occur at deeper depths (~35+ km), the uncertainty could become as large as 4–5 km (Emry et al., 2014). These estimates for uncertainty are on par with those suggested by prior studies (~3–5 km) (e.g. Taymaz et al., 1991; Tilmann et al., 2010; Craig et al., 2014).

3. Results

In total, we relocated 759 GCMT earthquakes and successfully inverted the waveforms of 63 earthquakes with Mw 5.2–7.4 (Table 1; Figs. 1–5, S4–S7). The results from waveform inversion for depth within the plate tend to be 1–5 km shallower than the original GCMT event depths for events in the 20–50 km depth range, likely due to the use of a specific source-side velocity model; however for events with GCMT depths fixed at 12–15 km, our final depth solutions range from less than 5 km to greater than 20 km beneath the seafloor (Fig. S2). We consider the waveform inversion depths to be more accurate than the GCMT depths because 1) the passband of our analysis extends to 0.5 Hz whereas the general GCMT analysis uses longer period waves, and higher frequencies are better able to resolve depth, 2) the depth of GCMT inversions are often necessarily fixed at 12 or 15 km due to poor depth resolution for shallow events resulting from use of only long period data, and 3) we compute our depths as the depth below the seafloor using 1-d local velocity models, which provides us with better information to place the event depth within the local structure by including the pP and sP reflections from the seabottom and the pwP water reverberation. A summary of the waveform inversion results is provided in Table 1. We find that, in general, our earthquake depths agree with new results from Craig et al. (2014), who use slightly different locations and a somewhat different approach to invert P- and SH-waveforms (Fig. S2).

To make our interpretation of incoming plate faulting as complete as possible, we include results from several previous studies that used waveform inversion methods to obtain accurate depths (Table S1). Most of these results come from several studies of pre-1990 incoming plate earthquakes using analog data from the WWSSN seismic network (e.g., Forsyth, 1982; Ward, 1983; Christensen and Ruff, 1988), and a few others include the depth range of faults as inferred from finite fault models of large events (Raeesi and Atakan, 2009; Lay et al., 2009).

4. Discussion

4.1. Depth extent of faulting within the incoming plate

The occurrence of incoming plate extensional earthquakes is variable along the ~13 000 km of the Northwest Pacific subduction zones during the ~20 yr record of good broadband global network coverage; however, we note that extensional earthquakes

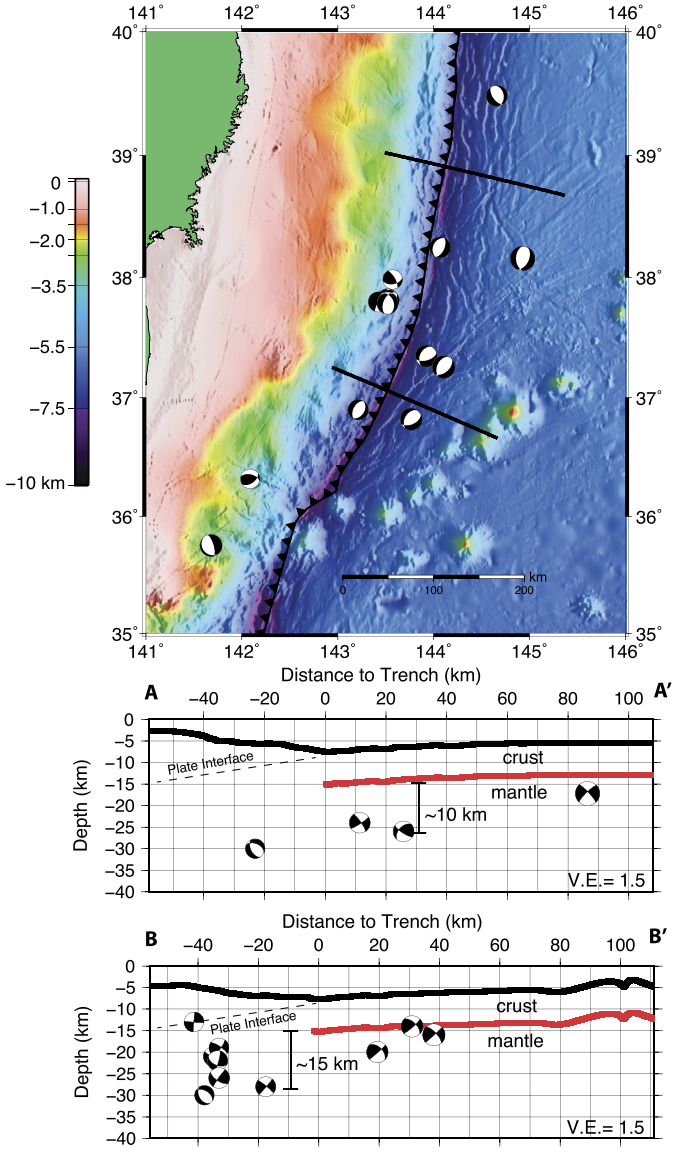

Fig. 4. Top: Map view of Northern Japan showing relocated earthquakes with newly determined depths. **Middle:** Cross-section along the northern Japan profile line showing the distance and depth of earthquakes in this study (colors and focal mechanisms are plotted as in Fig. 2). **Bottom:** Cross-section along the southern Japan profile line similar to above.

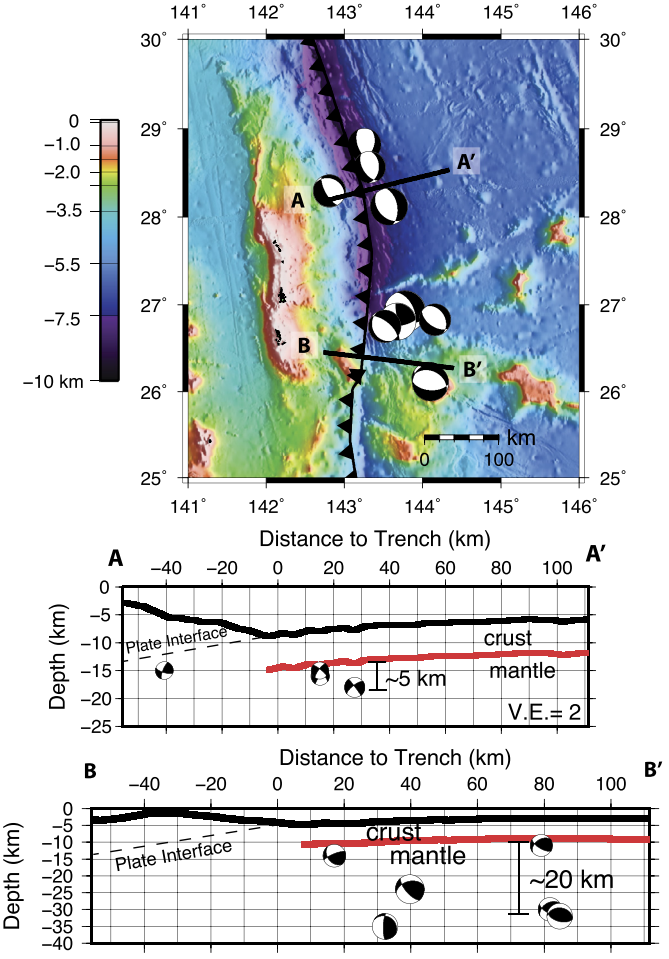

Fig. 5. Top: Map view of the Bonin Trench showing relocated earthquakes with newly determined depths. **Bottom:** Cross-section along the Northern Bonin profile line showing the distance and depth of earthquakes in this study (colors and focal mechanisms are plotted as in Fig. 2). **Bottom:** Cross-section along the Southern Bonin profile line similar to above.

occur in the incoming plate of every subduction zone down to at least 5 km within the mantle (Figs. 6, 7). In addition, most of the studied Pacific subduction zones have evidence for at least one extensional earthquake at ~10–15 km below the incoming plate moho. At the Western Aleutians and Southern Bonin trenches, extensional earthquakes occur even deeper, down to ~20 km below the top of the incoming plate mantle (Figs. 6, 7). Due to the short record of globally distributed broadband seismographs, the long-term pattern of incoming plate extensional earthquakes cannot be obtained; however after consideration of results from prior studies obtaining accurate event depths from waveform inversion or finite-fault modeling (Table S1, Fig. 7), it appears that extensional events at ~10–20 km below the moho although occurring less frequently, may be distributed more evenly throughout the entire length of the incoming plate in the Northwest Pacific. In comparison, the accurate depths determined in this study are predominantly shallower than the depths assigned to the shallowest GCMT events (Supplementary Fig. S8). If we had used GCMT depths for the shallowest incoming plate earthquakes, we would likely predict that the region of greatest serpentinization extends deeper into the incoming plate (down to 10 km instead of the 5 km suggested by our results) and thus would overpredict the amount of hydration brought into the subduction zone. Based on our ~20 yr earthquake distribution and results from previous studies, we postulate that pervasive faulting occurs globally within the top 5 km of the incoming plate mantle and that deeper extensional faulting occurs intermittently or discontinuously along the length of the Northern and Western Pacific subduction zones down to 10–20 km within the incoming plate mantle.

4.2. Variations in faulting and hydration with time and space

It is clear that the largest extensional incoming plate earthquakes can extend 25–30 km into the mantle, generally deeper than those observed in this study (e.g. Abe, 1972; Kanamori, 1972; Kao and Chen, 1996; Lynnes and Lay, 1988; Lay et al., 2009). It seems likely that these large incoming plate events are associated with temporal variations in stress and neutral plane depth within the incoming plate that result from the plate interface seismic cycle (Christensen and Ruff, 1983, 1988; Dmowska et al., 1988). After the great Tohoku plate interface earthquake, many extensional outer rise earthquakes occurred within the incoming plate at depths previously reported as compressional (Seno and Gonzalez, 1987; Hino et al., 2009; Gamage et al., 2009; Obana et al., 2012), which suggests that stresses within the in-

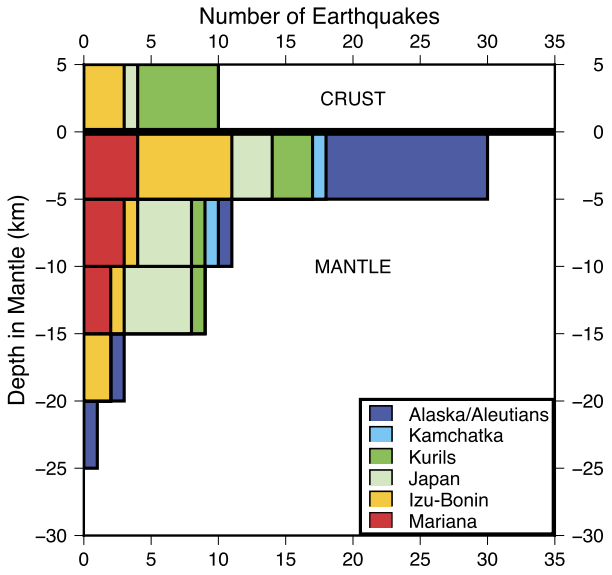

Fig. 6. Top: Histogram showing the number of extensional outer rise earthquakes occurring at each depth range: Crustal, 0–4 km below the moho, 5–9 km below the moho, 10–14 km below the moho, 15–19 km, and 20–24 km below the moho. Alaska and the Aleutians are shown in blue, Kamchatka is red, Kurils are shown in green, Japan is shown in purple, Izu–Bonin is light-blue, and Mariana (Emry et al., 2014) is orange. (For interpretation of the references to color in this figure legend, the reader is referred to the web version of this article.)

coming plate might be dependent upon the seismic cycle. These possible temporal variations of stress distributions within the incoming plate make it difficult to presume the long-term state of stress within the incoming plate, as some of our analyzed earthquakes followed great plate interface earthquakes. However, the plate interface seismic cycle may help to explain the lateral variations in maximum incoming plate event depth that we observe in this study, as different sections of the subduction zone may be at different stages of the seismic cycle, with recently ruptured regions showing the greatest event depths.

The extent to which the subduction plate interface seismic cycle might sway our results for incoming plate seismicity is not known. As discussed by Lefeldt et al. (2012), following active source seismic experiments in Central America, infrequent large extensional events may not be the best predictors of the depth of serpentinization; therefore it seems likely that the infrequent Mw 7+ events that occur within the incoming plate may be less important to mantle serpentinization than the general trend of Mw 5–6 events that we explore in our study. The event locations and depths determined in this paper, based on readily available teleseismic records, provide a useful first-order observation that extensional outer rise seismicity is prevalent throughout most of the Northwest Pacific subduction zones generally to a depth of at least 5 km below the moho, and deeper in some locations.

4.3. Water infiltration and storage in Pacific Oceanic mantle

We observe that extensional incoming plate faulting occurs at all subduction zones within at least the top 5 km, and in some places down to ~10–20 km within the incoming plate mantle. Nearly half of the extensional incoming plate events occur within the upper 5 km of the mantle, suggesting that the intensity of faulting is greater in the mantle than in the crust and that faulting decreases with depth below the uppermost mantle (Fig. 6). The deepest extensional incoming plate events are found at the Central and Western Aleutian Islands and at the Southern Bonin segment of the Izu–Bonin–Mariana subduction zone. Ranero et al. (2003) and Lefeldt et al. (2009) have suggested that the extensional incoming plate faults allow water to travel into the plate down to the

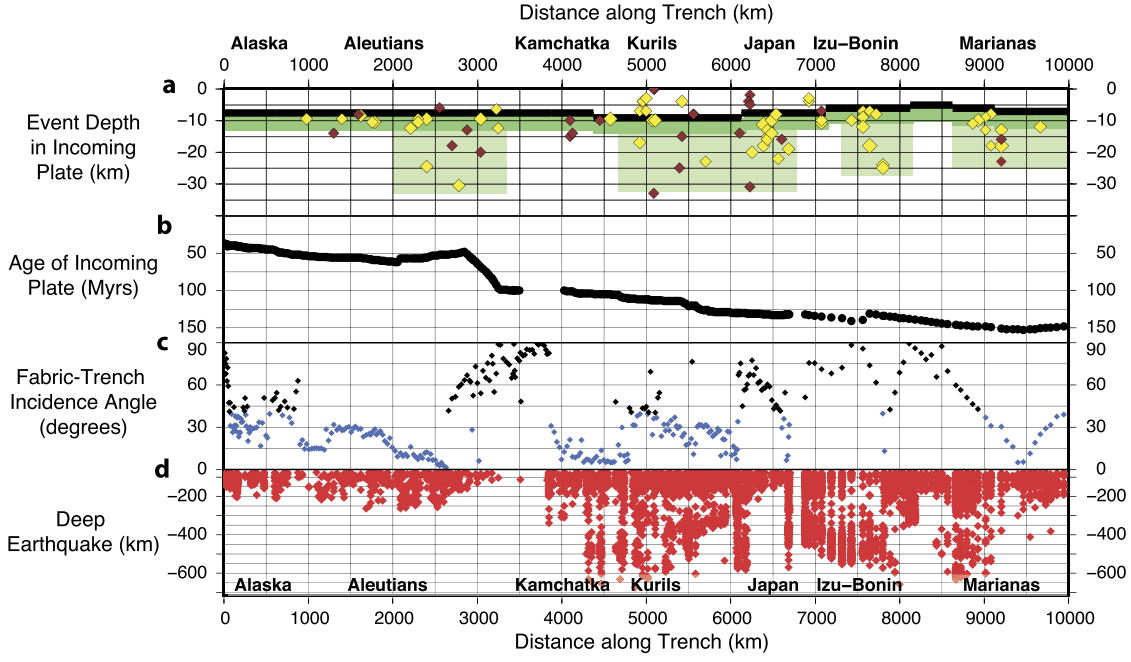

Fig. 7. Subduction zone processes and depth of outer rise faulting. (a) The depths of outer rise earthquakes versus the distance along the length of the entire North and Western Pacific subduction zones, starting at the eastern end of the Alaskan trench (0 km) to the southern end of the Mariana (Emry et al., 2014) trench (10 000 km). Earthquakes from this study are plotted as yellow diamonds and events from previous studies are plotted as dark red diamonds. (b). Incoming plate age (Myr) determined by Müller et al. (2008) was extracted using GEOMAPAPP and is plotted in the second window. (c) The fabric-trench incidence angle determined from the orientation of magnetic lineations (EMAG2) extracted using GEOMAPAPP and the orientation of the subduction trench axis. Seemingly spurious incidence angles are a result of small sections of the subduction trench axis that have significantly different orientations in comparison to the overall subduction zone. (d) Locations and depths of intermediate and deep slab earthquakes were extracted from the ISC bulletin (2010) plotted along the length of the margin. (For interpretation of the references to color in this figure legend, the reader is referred to the web version of this article.)

Table 2
Estimates for mantle hydration and subducted water.

Northwest Pacific plate mantle hydration scenario	Water input in mantle serpentinites[a] (10^8 Tg/Myr)	Total amount of input water[a,b] (10^8 Tg/Myr)
No mantle serpentinite (Van Keken et al., 2011)	0	1.5
Partial mantle serpentinite (Van Keken et al., 2011)	0.7	2.2
Full mantle serpentinite (Van Keken et al., 2011)	3.0	4.5
2 wt% in top 5 km of mantle	1.7	3.2
2 wt% in top 15 km of mantle	5.1	6.5
3.5 wt% in top 5 km of mantle	2.5	4.0
3.5 wt% in top 15 km of mantle	7.6	9.1
3 wt% to 5 km in mantle; 1 wt% to 15 km in mantle	4.2	5.7
3 wt% to 5 km; 1 wt% to 15 km along 1/2 of margin	3.4	4.9
2 wt% to 5 km; 0.5 wt% to 15 km along 1/4 of margin	1.9	3.4
Fig. 7: 2 wt% to 5 km; 0.5 wt% to depth specific to figure	2.9	4.4
Globally 2 wt% in top 5 km of mantle	7.9	14.8
Globally 3 wt% to 5 km in mantle; 1 wt% to 15 km in mantle	19.8	26.7
Globally 2 wt% to 5 km; 0.5 wt% to 15 km along 1/4 of margin	8.9	15.8

[a] All estimates shown are for the Northwest Pacific subduction zones, except the last three lines, which are global estimates.
[b] Estimates assume Van Keken et al. (2011) estimates of crustal contributions for subducted water.

depth of the neutral plane, hydrating dry ultramafic mantle materials, and active-source seismic surveys of the same region support this interpretation (Ivandic et al., 2008, 2010; Van Avendonk et al., 2011; Lefeldt et al., 2012). Active-source refraction surveys perpendicular to the trench axis show greater decrease in seismic velocity (increased serpentinization) within the incoming plate mantle as distance from the outer rise decreases (Contreras-Reyes et al., 2007; Ivandic et al., 2008, 2010); however prior to its arrival at the outer rise, some mantle serpentinization within the oceanic plate mantle may also occur at oceanic transform faults, hotspots, or slow-spreading mid-ocean ridges (e.g. Fryer, 2002; Gregg et al., 2007; Contreras-Reyes et al., 2008; Faccenda, 2014). Because serpentinites within the incoming plate are stable to greater than 600 °C at 5 GPa, water may be carried to significant depth in the subduction zone or may be carried beyond the subduction zone system and into the deeper mantle (Ulmer and Trommsdorf, 1995; Van Keken et al., 2011).

Uncertainty remains regarding the mechanism that allows water to be pulled into the incoming plate near the trench, as increasing lithostatic pressure at depth should prevent water from traveling downward into the plate (Sibson, 1994; Phipps Morgan and Holtzman, 2005; Korenaga, 2007; Faccenda et al., 2009). Regardless of the mechanism, experimental results reinforce the idea that serpentinization reactions within the incoming plate mantle should be primarily limited by availability of water (MacDonald and Fyfe, 1985).

The estimates of mantle serpentinization that are incorporated into numerical models of slab dehydration and water flux vary widely between authors. Van Keken et al. (2011) conservatively estimate the slab mantle as unserpentinized, partially serpentinized (2 wt% H_2O) down to 2 km, or fully saturated to 2 km. Hacker (2008) estimated the mantle to have 2 wt% H_2O down to 4 km; Schmidt and Poli (1998) assumes 5 km of mantle hydration with 10% average serpentinization; and Rüpke et al. (2004) assumed 10 km of upper mantle hydration. In our observations of extensional earthquake depths, it appears that no subduction zones have extensional faulting only at crustal depths within the incoming plate. Since all subduction zones that we studied show extensional faulting down to at least 5 km within the incoming plate mantle, we propose this as a lower bound estimate of the depth of slab hydration due to faulting. We do not calculate the water flux out of the subducting plate, as has been done in prior numerical models (e.g. Hacker, 2008; Van Keken et al., 2011; Wada et al., 2012), but rather make new estimates for the amount of water input into the subduction zones, which provide a useful comparison to the amounts previously assumed in the literature. Given the lower-bound scenario described above for plate mantle hydration, a moderate amount of serpentinization, and the parameters assumed by Van Keken et al. (2011) for the incoming plate motion and crustal hydration state, we would expect $\sim 3 \times 10^8$ Tg/Myr of water would be carried into the Northwestern Pacific subduction zones, or $\sim 15 \times 10^8$ Tg/Myr globally (Table 2).

A more realistic scenario might include some hydration deeper than 5 km within the mantle, because clearly a number of normal-faulting events occur at 10–20 km within the mantle. In addition, the largest observed incoming plate earthquakes involve ruptures propagating 20–30 km into the mantle. Given a scenario similar to above where a larger amount of hydration (3 wt%) extends to 5 km within the mantle and smaller amounts of hydration (1 wt%) extends to ~15 km into the mantle, we would expect $\sim 6 \times 10^8$ Tg/Myr of water would be input into the Northwestern Pacific subduction zones, or $\sim 26 \times 10^8$ Tg/Myr globally (Table 2).

4.4. Effect of laterally heterogeneous hydration within incoming plates

Based on the fact that some, but not all incoming plate regions show extensional earthquakes down to 10–20 km below the moho, as well as the lateral heterogeneity of mantle serpentinization and varying estimates for amount of slab mantle serpentinization at different locations ranging from 1–8 wt% H_2O (Holbrook et al., 1999; Carlson and Miller, 2003; Van Avendonk et al., 2011; Savage, 2012), we expect that the amount of serpentinite at deeper depths within the incoming plate is variable along the length of the subduction margin. A more specific estimate of hydration taking into account lateral variations in the depth of hydration based on the earthquake depths/locations determined in this study, and the assumption that the incoming plate mantle is partially serpentinized (0.5 wt% water) to depths specific to each subduction zone, gives an estimate of 4.4×10^8 Tg/Myr water carried into the Northwestern Pacific subduction zones. In this case the deepest hydration occurs in the Western and Central Aleutian, Kuril, Japan, Bonin, and Mariana subduction zones (Fig. 7, Table 2). If we extrapolate a similar estimate for heterogeneous lateral hydration in the Northwestern Pacific subduction zones to the rest of the Earth's subduction zones, then we anticipate that globally ~ 14–16×10^8 Tg/Myr of water is input into the Earth's subduction zones (Table 2). For comparison, this amount is 1.5 times greater than estimated by Van Keken et al. (2011), slightly larger than Hacker (2008), 2 times larger than Jarrard (2003), and within the range estimated by Rüpke et al. (2004). Furthermore, some regions may have notably higher water concentrations (i.e. 4–8 wt%

in Nicaragua, Tonga) than the estimate we provide above, and so our calculation above is likely on the conservative end (Van Avendonk et al., 2011; Savage, 2012).

Similar to the Nicaragua–Costa Rica outer rise, it is likely that hydration in the incoming plate is distributed heterogeneously along length of subduction zones, with greater amounts of water subducted in some regions (Van Avendonk et al., 2011). At Nicaragua, evidence for deep mantle serpentinization coincided with regions where incoming plate fabric was parallel to the subduction trench axis, and only minor mantle serpentinization was found where minimal outer rise faulting was identified (Ranero et al., 2005; Van Avendonk et al., 2011); it has thus been proposed that plate fabric impacts the extent of outer rise faulting (Ranero et al., 2005).

In order to explore this and other factors that have been suggested to affect or to be dependent upon plate faulting and hydration, we plot incoming plate earthquake depths and locations along the length of the northwestern Pacific subduction zones alongside incoming plate age, seafloor fabric, and intermediate and deep earthquakes (Fig. 7). As demonstrated by Fig. 7, we find no significant correlation between the distribution of outer rise extensional faulting and other subduction zone characteristics. For instance, although 100+ Ma plate age appears to coincide well with the region of deep outer rise earthquakes in the Western Pacific, the Western and Central Aleutians also have deep outer rise earthquakes, and the age of the incoming plate in this region is ~50 Ma (Müller et al., 2008). Similarly, no obvious relationship appears to exist between intermediate/deep earthquakes and faults in the incoming plate; intermediate depth earthquakes appear to occur at similar depths throughout the Aleutians despite a pronounced difference in outer rise extensional earthquakes (ISC bulletin, 2010). Incoming plate fabric is generally nearly parallel to the trench axis along regions where deep extensional earthquakes occur within the incoming plate, however several regions exist where this relationship does not hold (EMAG2, www.geomapapp.org). Therefore, it appears that the age, plate fabric, and intermediate depth slab earthquake relationships that have been previously proposed do not correlate well with the occurrence of moderately-sized incoming plate earthquakes as determined in this paper.

4.5. Implications to global water budgets

The results of this study show that the depths of northwest Pacific earthquakes, together with observed links between depths of faulting and hydration of the incoming plate, suggest that estimates of the amount of water entering the mantle need to be revised upward. This result is in stark contrast with a recent model of the Earth's water budget that uses slab water flux models, volcanic outputs, and estimates of global sealevel during the Phanerozoic to constrain the maximum amount of water that is brought into the subduction zone (Parai and Mukhopadhyay, 2012). Parai and Mukhopadhyay (2012) suggest that even the conservative estimates of Van Keken et al. (2011) overestimate the amount of water input into subduction zones globally. Our results presented in this paper have an even larger discrepancy with the estimates of Parai and Mukhopadhyay (2012).

If we assume that, as concluded by Parai and Mukhopadhyay (2012), much less water needs to be input into subduction zones in order to match the constraints provided by previous studies, then this could lead us to conclude that either extensional faulting within the outer rise does not promote mantle serpentinization, that we cannot extrapolate our inferred distribution of hydration from the Northwestern Pacific to other subduction zones, or that we cannot extrapolate the distribution through deep time. We do not attempt to address the validity of assuming extrapolation to deep time in this paper.

However, as discussed earlier, the correlation between hydration patterns inferred from active source refraction surveys and distribution of extensional earthquakes (e.g. Lefeldt et al., 2009; Van Avendonk et al., 2011) supports the connection we assume between extensional earthquake depth and hydration. Additionally, the depth and distribution of hydration observed at the Nicaragua and Costa Rica margin is similar to what we expect to see throughout the regions we have focused on in this paper. Furthermore, given the broad range of incoming plate mantle water contents inferred in various locations (1–8 wt%) (Holbrook et al., 1999; Van Avendonk et al., 2011; Savage, 2012), we suggest that it is reasonable to extrapolate our Northwestern Pacific estimates, which assume 1–3 wt% H_2O, to the rest of the globe. We anticipate that at some subduction zones we may significantly underestimate or in some places slightly overestimate the amount of water within the incoming plate mantle.

One possible partial solution to the discrepancies between the Parai and Mukhopadhyay (2012) conclusions with prior studies and our conclusions (e.g., Hacker, 2008; Van Keken et al., 2011) was outlined by Wada et al. (2012), who show that the assumption of homogeneously distributed hydration in most models of slab water flux is likely not realistic. Given a down-going slab with hydration localized along faults, the rate of shallow water expulsion from the slab increases and the maximum depth at which water is expelled from the slab decreases. Wada et al. (2012) suggest that this effect would cause more water from the slab to be liberated in the forearc and arc regions, which would decrease the amount of water subducted into the deeper mantle and partially alleviate some discrepancies between the global water budget and estimates for incoming plate hydration. In addition to refinements to slab water flux models, some have called into question the reliability of using olivine-hosted melt inclusions to determine pre-eruptive water contents of the subduction zone mantle wedge as well as to infer the magma degassing path (e.g. Gaetani et al., 2012; Bucholz et al., 2013; Plank et al., 2013; Esposito et al., 2014). It appears that our estimates of water within the incoming plate are reasonable given the range observed in other studies (e.g., Van Avendonk et al., 2011; Savage, 2012). If these higher estimates cannot be reconciled by effect of localized hydration on slab water flux (Wada et al., 2012) or by uncertainty regarding Earth's water outputs (e.g., Plank et al., 2013), then it would require that the Earth's mantle is accumulating water at a greater rate than concluded by Parai and Mukhopadhyay (2012).

5. Conclusion

We explored extensional and compressional outer rise earthquakes at Northern and Western Pacific subduction zones in order to estimate the depth at which extensional faulting may allow water to infiltrate into and serpentinize dry mantle rocks prior to subduction. We relocated and analyzed teleseismic P- and SH-waveforms of 63 subduction zone outer rise and trench earthquakes ranging from Mw 5.2–7.4, and we find that the mantle at most Northern and Western Pacific subduction zone outer rises exhibits extensional faulting to depths of ~15 km, with the highest concentration of extensional events extending down to ~5 km below the crust. We observe some regional variation between the different subduction zones, and we observe some variation along the length of individual subduction zones; however the length of the seismic record is short (~20 yr), and regional variations may not be consistent through time. If the top ~5 km of mantle is pervasively faulted & hydrated (~2 wt% H_2O) and if the mantle down to ~15 km is intermittently faulted and hydrated (~0.5 wt% H_2O), then our lower bound estimates for water input into the Northern and Western Pacific subduction zones would be $\sim 5 \times 10^8$ Tg/Myr; extrapolated globally this would result in

$\sim 15 \times 10^8$ Tg/Myr, which is towards the larger end of previous estimates.

Acknowledgements

Thank you to C. Ammon, M. Brounce, H. Chou, G. Euler, K. Furlong, M. Herman, K. Kelley, P. LaFemina, B. Shiro, P. Shore, S. Solomatov, and L. Warren for discussion and technical assistance. Thank you to editor P. Shearer, B. Savage, and one anonymous reviewer whose helpful reviews improved this paper and are very appreciated. The IRIS Data Management Center provided access to all of the waveform data used in this study. Support for this research was provided under grants OCE-0426408, OCE-0752476, and OCE-0841074 as well as the NSF Earth Sciences postdoctoral fellowship (grant EAR-1349684). Funding to present this research was also provided by the NSF Earthscope, GeoPRISMs, and the CIDER II program (EAR-1135452). Maps and cross-sections were created using the GMT software (Wessel and Smith, 1991). Data for oceanic plate age and seafloor magnetic anomalies were extracted from EMAG2 using the GeoMapApp program (www.geomapapp.org). Programs to compute SNR came from the SEIZMO MATLAB programs, courtesy of G. Euler (github.com/g2e/seizmo).

Appendix A. Supplementary material

Supplementary material related to this article can be found online at http://dx.doi.org/10.1016/j.epsl.2014.12.042.

References

Abe, K., 1972. Lithospheric normal faulting beneath the Aleutian trench. Phys. Earth Planet. Inter. 5, 190–198. http://dx.doi.org/10.1016/0031-9201(72)90091-X.

Bucholz, C.E., Gaetani, G.A., Behn, M.D., Shimizu, N., 2013. Post-entrapment modification of volatiles and oxygen fugacity in olivine-hosted melt inclusions. Earth Planet. Sci. Lett. 374, 145–155. http://dx.doi.org/10.1016/j.epsl.2013.05.033.

Carlson, R.L., Miller, D.J., 2003. Mantle wedge water contents estimated from seismic velocities in partially serpentinized peridotites. Geophys. Res. Lett. 30 (5), 1250. http://dx.doi.org/10.1029/2002GL016600.

Christensen, D.H., Ruff, L.J., 1983. Outer-rise earthquakes and seismic coupling. Geophys. Res. Lett. 10 (8), 697–700. http://dx.doi.org/10.1029/GL010i008p00697.

Christensen, D.H., Ruff, L.J., 1988. Seismic coupling and outer rise earthquakes. J. Geophys. Res. 93 (B11), 13421–13444. http://dx.doi.org/10.1029/JB093iB11p13421.

Contreras-Reyes, E., Grevemeyer, I., Flueh, E.R., Scherwath, M., Heesemann, M., 2007. Alteration of the subducting oceanic lithosphere at the Southern Central Chile trench-outer rise. Geochem. Geophys. Geosyst. 8 (7), Q07003. http://dx.doi.org/10.1029/2007GC001632.

Contreras-Reyes, E., Grevemeyer, I., Flueh, E.R., Scherwath, M., Bialas, J., 2008. Effect of trench-outer rise bending-related faulting on seismic Poisson's ratio and mantle anisotropy: a case study offshore of Southern Central Chile. Geophys. J. Int. 173, 142–156. http://dx.doi.org/10.1111/j.1365-246X.2008.03716.x.

Craig, T.J., Copley, A., Jackson, J., 2014. A reassessment of outer-rise seismicity and its implications for the mechanics of oceanic lithosphere. Geophys. J. Int. 197, 63–89. http://dx.doi.org/10.1093/gji/ggu013.

Crotwell, H.P., Owens, T.J., Ritsema, J., 1999. The TauP Toolkit: flexible seismic traveltime and ray-path utilities. Seismol. Res. Lett. 70, 154–160. http://dx.doi.org/10.1785/gssrl.70.2.154.

Dmowska, R., Rice, J.R., Lovison, L.C., Josell, D., 1988. Stress transfer and seismic phenomena in coupled subduction zones during the earthquake cycle. J. Geophys. Res. 93 (B7), 7869–7884. http://dx.doi.org/10.1029/JB093iB07p07869.

Emry, E.L., Wiens, D.A., Garcia-Castellanos, D., 2014. Faulting within the Pacific Plate at the Mariana Trench: implications for plate interface coupling and subduction of hydrous minerals. J. Geophys. Res. 119. http://dx.doi.org/10.1002/2013JB010718.

Esposito, R., Hunter, J., Schiffbauer, J.D., Shimizu, N., Bodnar, R.J., 2014. An assessment of the reliability of melt inclusions as recorders of the pre-eruptive volatile content of magmas. Am. Mineral. 99, 976–998. http://dx.doi.org/10.2138/am.2014.4574.

Faccenda, M., Gerya, T.V., Burlini, L., 2009. Deep slab hydration induced by bending-related variations in tectonic pressure. Nat. Geosci. 2, 790–793. http://dx.doi.org/10.1038/NGEO656.

Faccenda, M., 2014. Water in the slab: a trilogy. Tectonophysics 614, 1–30. http://dx.doi.org/10.1016/j.tecto.2013.12.020.

Forsyth, D.W., 1982. Determinations of focal depths of earthquakes associated with the bending of oceanic plates at trenches. Phys. Earth Planet. Inter. 28 (2), 141–160. http://dx.doi.org/10.1016/0031-9201(82)90079-6.

Fryer, P., 2002. Recent studies of serpentinite occurrences in the oceans: mantle–ocean interactions in the plate tectonic cycle. Chem. Erde 62, 257–302.

Gaetani, G.A., O'Leary, J.A., Shimizu, N., Bucholz, C.E., Newville, M., 2012. Rapid reequilibration of H_2O and oxygen fugacity in olivine-hosted melt inclusions. Geology 40 (10), 915–918. http://dx.doi.org/10.1130/G32992.1.

Gamage, S.S.N., Umino, N., Hasegawa, A., Kirby, S.H., 2009. Offshore double-planed shallow seismic zone in the NE Japan forearc region revealed by sP depth phases recorded by regional networks. Geophys. J. Int. 178, 195–214. http://dx.doi.org/10.1111/j.1365-246X.2009.04048.x.

Gregg, P.M., Lin, J., Behn, M.D., Montési, L.G.J., 2007. Spreading rate dependence of gravity anomalies along oceanic transform faults. Nature 448, 183–187. http://dx.doi.org/10.1038/nature05962.

Hacker, B.R., 2008. H_2O subduction beyond arcs. Geochem. Geophys. Geosyst. 9, Q03001. http://dx.doi.org/10.1029/2007GC001707.

Hino, R., Azuma, R., Ito, Y., Yamamoto, Y., Suzuki, K., Tsushima, H., Suzuki, S., Miyashita, M., Tomori, T., Arizono, M., Tange, G., 2009. Insight into complex rupturing of the immature bending normal fault in the outer slope of the Japan Trench from aftershocks of the 2005 Sanriku earthquakes (Mw = 7.0) located by ocean bottom seismometry. Geochem. Geophys. Geosyst. 10 (7), Q07O18. http://dx.doi.org/10.1029/2009GC002415.

Hirschmann, M.M., 2006. Water, melting, and the deep Earth H_2O cycle. Annu. Rev. Earth Planet. Sci. 34, 629–653. http://dx.doi.org/10.1146/annurev.earth.34.031405.125211.

Holbrook, W.S., Lizarralde, D., McGeary, S., Bangs, N., Diebold, J., 1999. Structure and composition of the Aleutian island arc and implications for continental crustal growth. Geology 27 (1), 31–34. http://dx.doi.org/10.1130/0091-7613(1999)027<0031:SACOTA>2.3.CO;2.

International Seismological Centre, 2010. On-line bulletin, http://www.isc.ac.uk, Internatl. Seis. Cent., Thatcham, United Kingdom.

Ivandic, M., Grevemeyer, I., Berhorst, A., Flueh, E.R., McIntosh, K., 2008. Impact of bending related faulting on the seismic properties of the incoming oceanic plate offshore of Nicaragua. J. Geophys. Res. 113, B05410. http://dx.doi.org/10.1029/2007JB005291.

Ivandic, M., Grevemeyer, I., Bialas, J., Petersen, C.J., 2010. Serpentinization in the trench-outer rise region offshore of Nicaragua: constraints from seismic refraction and wide-angle data. Geophys. J. Int. 180, 1253–1264. http://dx.doi.org/10.1111/j.1365-246X.2009.04474.x.

Jarrard, R.D., 2003. Subduction fluxes of water, carbon dioxide, chlorine, and potassium. Geochem. Geophys. Geosyst. 4 (5), 8905. http://dx.doi.org/10.1029/2002GC000392.

Jordan, T.H., Sverdrup, K.A., 1981. Teleseismic location techniques and their application to earthquake clusters in the South-Central Pacific. Bull. Seismol. Soc. Am. 71 (4), 1105–1130.

Kanamori, H., 1971. Seismological evidence for a lithospheric normal faulting—the Sanriku earthquake of 1933. Phys. Earth Planet. Inter. 4, 289–300. http://dx.doi.org/10.1016/0031-9201(71)90013-6.

Kanamori, H., 1972. Mechanism of tsunami earthquakes. Phys. Earth Planet. Inter. 6, 346–359. http://dx.doi.org/10.1016/0031-9201(72)90058-1.

Kao, H., Chen, W.-P., 1996. Seismicity in the outer rise-forearc region and configuration of the subducting lithosphere with special reference to the Japan Trench. J. Geophys. Res. 101 (B12), 27,811–27,831. http://dx.doi.org/10.1029/96JB01760.

Kelley, K.A., Plank, T., Grove, T.L., Stolper, E.M., Newman, S., Hauri, E., 2006. Mantle melting as a function of water content beneath back-arc basins. J. Geophys. Res. 111, B09208. http://dx.doi.org/10.1029/2005JB003732.

Kennett, B.L.N., Engdahl, E.R., 1991. Traveltimes for global earthquake location and phase identification. Geophys. J. Int. 105 (2), 429–465. http://dx.doi.org/10.1111/j.1365-246X.1991.tb06724.x.

Korenaga, J., 2007. Thermal cracking and the deep hydration of oceanic lithosphere: a key to the generation of plate tectonics? J. Geophys. Res. 112, B05408. http://dx.doi.org/10.1029/2006JB004502.

Langston, C.A., Helmberger, D.V., 1975. A procedure for modeling shallow dislocation sources. Geophys. J. R. Astron. Soc. 42 (1), 117–130. http://dx.doi.org/10.1111/j.1365-246X.1975.tb05854.x.

Lay, T., Kanamori, H., Ammon, C.J., Hutko, A.R., Furlong, K., Rivera, L., 2009. The 2006–2007 Kuril Islands great earthquake sequence. J. Geophys. Res. 114, B11308. http://dx.doi.org/10.1029/2008JB006280.

Lefeldt, M., Grevemeyer, I., Goßler, J., Bialas, J., 2009. Intraplate seismicity and related mantle hydration at the Nicaraguan trench outer rise. Geophys. J. Int. 178 (2), 742–752. http://dx.doi.org/10.1111/j.1365-246X.2009.04167.x.

Lefeldt, M., Ranero, C.R., Grevemeyer, I., 2012. Seismic evidence of tectonic control on the depth of water influx into incoming oceanic plates at subduction trenches. Geochem. Geophys. Geosyst. 13 (5), Q05013. http://dx.doi.org/10.1029/2012GC004043.

Lynnes, C.S., Lay, T., 1988. Source process of the great 1977 Sumba earthquake. J. Geophys. Res. 93 (B11), 13407–13420. http://dx.doi.org/10.1029/JB093iB11p13407.

MacDonald, A.H., Fyfe, W.S., 1985. Rate of serpentinization in seafloor environments. Tectonophysics 116, 123–135. http://dx.doi.org/10.1016/0040-1951(85)90225-2.

Müller, R.D., Sdrolias, M., Gaina, C., Roest, W.R., 2008. Age, spreading rates, and spreading asymmetry of the world's ocean crust. Geochem. Geophys. Geosyst. 9 (4), Q04006. http://dx.doi.org/10.1029/2007GC001743.

Obana, K., Fujie, G., Takahashi, T., Yamamoto, Y., Nakamura, Y., Kodaira, S., Takahashi, N., Kaneda, Y., Shinohara, M., 2012. Normal-faulting earthquakes beneath the outer slope of the Japan Trench after the 2011 Tohoku earthquake: implications for the stress regime in the incoming Pacific plate. Geophys. Res. Lett. 39, L00G24. http://dx.doi.org/10.1029/2011GL050399.

Parai, R., Mukhopadhyay, S., 2012. How large is the subducted water flux? New constraints on mantle regassing rates. Earth Planet. Sci. Lett. 317, 396–406. http://dx.doi.org/10.1016/j.epsl.2011.11.024.

Phipps Morgan, J., Holtzman, B.K., 2005. Vug waves: a mechanism for coupled rock deformation and fluid migration. Geochem. Geophys. Geosyst. 6 (8), Q08002. http://dx.doi.org/10.1029/2004GC000818.

Plank, T., Kelley, K.A., Zimmer, M.M., Hauri, E.H., Wallace, P.J., 2013. Why do mafic magmas contain ~4 wt% water on average? Earth Planet. Sci. Lett. 364, 168–179. http://dx.doi.org/10.1016/j.epsl.2012.11.044.

Raeesi, M., Atakan, K., 2009. On the deformation cycle of a strongly coupled plate interface: the triple earthquakes of 16 March 1963, 15 November 2006, and 13 January 2007 along the Kurile subduction zone. J. Geophys. Res. 114, B10301. http://dx.doi.org/10.1029/2008JB006184.

Ranero, C.R., Phipps Morgan, J., McIntosh, K., Reichert, C., 2003. Bending-related faulting and mantle serpentinization at the Middle America trench. Nature 425 (6956), 367–373. http://dx.doi.org/10.1038/nature01961.

Ranero, C.R., Villasenor, A., Morgan, J.P., Weinrebe, W., 2005. Relationship between bend-faulting at trenches and intermediate-depth seismicity. Geochem. Geophys. Geosyst. 6 (12), Q12002. http://dx.doi.org/10.1029/2005GC000997.

Rüpke, L.H., Phipps Morgan, J., Hort, M., Connolly, J.A.D., 2004. Serpentine and the subduction zone water cycle. Earth Planet. Sci. Lett. 223 (1–2), 17–34. http://dx.doi.org/10.1016/j.epsl.2004.04.018.

Savage, B., 2012. Seismic constraints on the water flux delivered to the deep Earth by subduction. Geology 40 (3), 235–238. http://dx.doi.org/10.1130/G32499.1.

Schmidt, M.W., Poli, S., 1998. Experimentally based water budgets for dehydrating slabs and consequences for arc magma generation. Earth Planet. Sci. Lett. 163 (1–4), 361–379. http://dx.doi.org/10.1016/S0012-821X(98)00142-3.

Seno, T., Gonzalez, D.G., 1987. Faulting caused by earthquakes beneath the outer slope of the Japan trench. J. Phys. Earth 35, 381–407.

Sibson, R.H., 1994. Crustal stress, faulting and fluid flow. In: Parnell, J. (Ed.), Geofluids: Origin, Migration and Evolution of Fluids in Sedimentary Basins. In: Geo. Society. Spec. Pub., vol. 78. Geological Society, London, pp. 69–84.

Taymaz, T., Jackson, J., McKenzie, D., 1991. Active tectonics of the north and central Aegean Sea. Geophys. J. Int. 106, 433–490. http://dx.doi.org/10.1111/j.1365-246X.1991.tb03906.

Tilmann, F.J., Craig, T.J., Grevemeyer, I., Suwargadi, B., Kopp, H., Flueh, E., 2010. The updip seismic/aseismic transition of the Sumatra megathrust illuminated by aftershocks of the 2004 Aceh-Andaman and 2005 Nias events. Geophys. J. Int. 181, 1261–1274. http://dx.doi.org/10.1111/j.1365-246X.2010.04597.x.

Ulmer, P., Trommsdorf, V., 1995. Serpentine stability to mantle depths and subduction-related magmatism. Science 268 (5212), 858–861. http://dx.doi.org/10.1126/science.268.5212.858.

Van Avendonk, H.J.A., Holbrook, W.S., Lizarralde, D., Denyer, P., 2011. Structure and serpentinization of the subducting Cocos plate offshore Nicaragua and Costa Rica. Geochem. Geophys. Geosyst. 12, Q06009. http://dx.doi.org/10.1029/2011GC003592.

Van Keken, P.E., Hacker, B.R., Syracuse, E.M., Abers, G.A., 2011. Subduction factory: 4. Depth-dependent flux of H_2O from subducting slabs worldwide. J. Geophys. Res. 116, B01401. http://dx.doi.org/10.1029/2010JB007922.

Wada, I., Behn, M.D., Shaw, A.M., 2012. Effects of heterogeneous hydration in the incoming plate, slab rehydration, and mantle wedge hydration on slab-derived H_2O flux in subduction zones. Earth Planet. Sci. Lett. 353, 60–71. http://dx.doi.org/10.1016/j.epsl.2012.07.025.

Ward, S.N., 1983. Body wave inversion: moment tensors and depths of oceanic intraplate bending earthquakes. J. Geophys. Res. 88. http://dx.doi.org/10.1029/JB080i011p09315.

Wessel, P., Smith, W.H.F., 1991. Free software helps map and display data. Eos Trans. AGU 72, 441.